Advanced Physics Laboratory

Electro- & Photoluminescense in Semiconductors

Name: Nicolò De Masi, Manthan Chattopadhyay

Experiment Date: 16.04.2024

Abstract

This lab investigates optical properties of various semiconductor devices. Luminescence spectra of five diodes were recorded to determine parameters such as exciton binding energy, band gap and doping ratio. A room temperature study of the luminescence band of an infrared-emitting GaAs diode was used to determine ionization energies of donors and acceptors. Lastly, two unintentionally doped $Ga_{1-x}Al_xAs$ samples were studied to discuss temperature dependence of such parameters.

Contents

1 Theoretical Background **4**
- 1.1 The Band Model . . . 4
- 1.2 Defects and Doping . . . 5
- 1.3 P-n junction . . . 6
- 1.4 Electroluminescence of Diodes at Room Temperature . . . 7
  - 1.4.1 White-emitting diodes . . . 7
  - 1.4.2 Infrared-emitting GaAs Diode . . . 7
  - 1.4.3 Red-emitting Ga(As, P) Diode . . . 8
  - 1.4.4 Yellow-emitting Ga(As, P) Diode . . . 9
  - 1.4.5 Green-emitting GaP diode . . . 9
  - 1.4.6 Blue-emitting SiC diode . . . 10
- 1.5 Photoluminescence of $Ga_{1-x}Al_xAs$ sample . . . 10

2 Experimental Setup **11**

3 Results & Discussion **14**
- 3.1 Emission Spectra of Sodium . . . 14
  - 3.1.1 597 nm lines . . . 14
  - 3.1.2 819 nm lines . . . 15
  - 3.1.3 497 nm lines . . . 16
- 3.2 Luminescence Spectra of a White Light Emitting Diode . . . 16
- 3.3 Luminescence Spectra of a Blue Light Emitting Diode . . . 17
- 3.4 Luminescence Spectra of a Green Light Emitting Diode . . . 18
- 3.5 Luminescence Spectra of a Yellow Light Emitting Diode . . . 19
- 3.6 Luminescence Spectra of a Red Light Emitting Diode . . . 20
- 3.7 Luminescence Spectra of an Infrared Light Emitting Diode . . . 22
- 3.8 Temperature Dependent Luminescence Spectra of Two AlGaAs Samples . . . 24

4 Conclusion & Outlook **29**

1 Theoretical Background

1.1 The Band Model

Our main focus is the study of crystalline semiconductors which due to their periodic arrangement of atoms, subject valence electrons to a potential of the following form:

$$V(x) = V(x + a) \tag{1}$$

where a is the lattice constant. The potential is due to the effect of the ion cores in the lattice and all other electrons [1]. According to Bloch's theorem, the eigenstates ψ of a one particle Hamiltonian in a potential of the form in (1) is a product of plane waves and a lattice periodic function $u_k(x)$ such that

$$\psi_k(x) = u_k(x)e^{ikx} \tag{2}$$

where $k = \frac{2\pi}{\lambda}$ is the wavenumber. Adding a perturbative term to the tight binding model [2,3] the solution to the Schrödinger equation yields the following energy eigenvalues:

$$E_n = E_n^{\text{atom}} - C - 2A_n \cos(ka) \tag{3}$$

E_n^{atom} is the atomic energy eigenvalues and $C > 0$ the perturbation of the atomic potential due to the lattice. A_n depends on the overlap of electron wave functions and the cosine term is the so-called exchange energy. It encodes the fact that valence electrons lose their 'atomic parent' in the lattice and can be situated at any atom with equal probability. Thus, equation (3) states that the discrete atomic energy levels transform into a energy continuum in a crystal - an energy band.
In order to take into account the effect of the lattice on the electrons, we introduce the effective mass m_{eff} which is analogous to free particles and is defined as $1/m_{eff} = \partial_k^2 E(k)/\hbar$. Since the electrons near the Γ point ($k = 0$) are mostly excited, we can approximate the cosine function in (3) with its first Taylor term

$$E \approx C' + Ak^2a^2 = C' + \frac{\hbar^2 k^2}{2m_{eff}} \tag{4}$$

where $C' = E_n^{\text{atom}} - C - 2A_n$. We thus have a splitting of the discrete atomic spectrum into energy bands of the crystal lattice with the same quadratic dependency as for the free electron.

In semiconductors, only electrons in the valence band and the conduction band determine a material's ability to properly conduct or absorb electrons. The band gap present between the two (Figure 1) is such that an electron with sufficient energy can "jump" from one to the other.

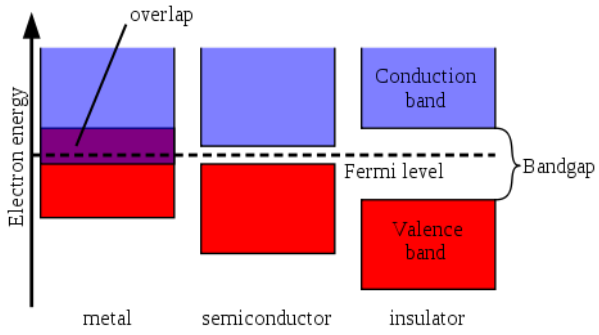

Figure 1: Illustration of different band gaps for different type of materials

Semiconductors can be further differentiated into direct and indirect [4], entirely based on the position of the maxima of the valence band, and the minima of the conduction band. An aligned wave-number k between the two levels means that an electron will be able to maintain the same momentum $p = \hbar k$, whilst for a different k, momentum is not conserved, as such, another particle (a phonon) must be present to collide with the electron, change its momentum and allow the transition to take place. We will deal with both direct and indirect semiconductors.

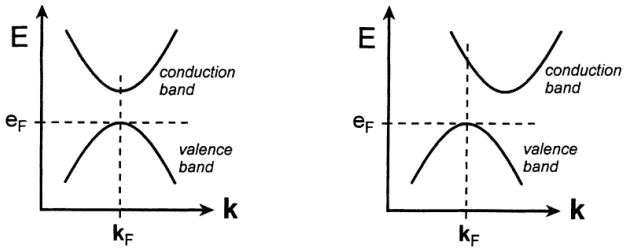

Figure 2: Illustration of the bandgap for Directs(left) and Indirects(right) semiconductors

1.2 Defects and Doping

The periodic lattice structure of crystals allows for predictable behavior that can, in many cases, be exploited by purposely incorporating other substances to a certain semiconductor. This process is called doping, where the aim is to enhance the response of the material to a manufacturer's liking. Deviations from the ideal structure are called defects [1]. The effect that these defects have on the general electric behaviour are determined by the number of valence electrons that the new element has in comparison to the original one.

- If the new element has more valence electrons than the element it is replacing, we call it a **Donor**, as the extra electron(s) can be easily transferred to the lattice, with a correspond ionization energy of [4]:

$$E_{donor} = \frac{E_H m_n}{\epsilon^2 m} \tag{5}$$

Here the effective mass m_n refers to an electron, whilst E_H is the binding energy in the hydrogen atom ($E_H = 13.6eV$)

- If it has less valence electrons then the original element, an electron of the original lattice can easily be trapped by the "hole" in the new atom, thus behaving as an **Acceptor** of sort. This time its ionization energy will correspond to [4]:

$$E_{acceptor} = \frac{E_H m_p}{\epsilon^2 m} \tag{6}$$

With m_p being the negative effective mass of a hole.

- Lastly, we talk about the case in which the doping substance has the same number of valence electrons (making the defect electrically neutral), but a different ionic radius. This will alter the binding energies, which in turn will originate a potential well, possibly trapping an electron-hole pair. This phenomena is called an **isoelectronic** defect. The electron-hole pair (exciton) will have an ionization energy of [4]:

$$E_{ex} = \frac{E_H \mu}{\epsilon^2 m_n} \tag{7}$$

With μ being the reduced mass of the exciton: $\frac{1}{\mu} = \frac{1}{m_n} + \frac{1}{m_p}$

In our experiments we deal with samples that present the behavior of each different type of doping.

1.3 P-n junction

An overview of the structure of the diodes we are going to use is necessary. The photo-luminescence effect is the principle via which these diodes convert electrical energy into radiation. This phenomena is possible because of the sample being composed of two semiconductors: an **n-type** region, so called because of a high concentration of donors, and as such with more electrons than empty holes, and a **p-type** region, with opposite conditions. The p-n junction is the boundary between these two distinct sections. Due to the two areas having opposite Fermi levels(close to the conduction band in the n-type, while in the p-region it is closer to the valence band), their junction results in a region of the semiconductor with a steep potential drop. An anode connected to the p-type region and a cathode connected to the n-type, will cause the electric current to flow uniquely in one direction with a lower resistivity. We will now have additional electrons reaching the p-region and more holes in the n-region(**injection**). The potential barrier of the junction will get reduced by the applied bias eV. This will increase the intensity of the recombination between holes and electrons, which is the origin of the emission of radiation. In this new non-equilibrium state, the Fermi level will shift between the energies of the two regions, yielding two quasi-Fermi levels such that:

$$E_{F_n} - E_{F_p} = eV \tag{8}$$

1.4 Electroluminescence of Diodes at Room Temperature

Within a given sample, different types of recombination events may take place that lead to emission of different wavelengths.

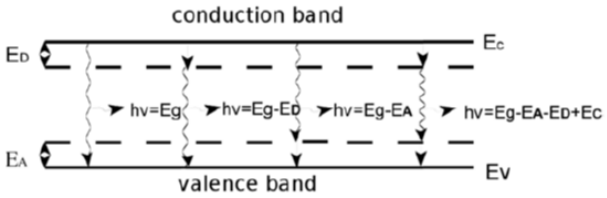

Figure 3: Recombination Events (from left to right): Band-to-Band, Donor-to-Band, Band-to-Acceptor (collectively called Impurity-to-Band), Pair-Recombination [4]

1.4.1 White-emitting diodes

White light is a combination of multiple wavelengths of light. In the context of manufacturing, there are multiple ways of achieving a white emission:

- Colour mixing: Multiple diodes of primary colours such as red, green and blue are used to produce di-, tri-, and tetra-chromatic white LEDs. An emission spectra analysis may yield distinct peaks throughout the visible spectrum [5].
- Phosphor converting: Blue or near-UV diodes are used to to excite a phosphor powder that in turn emits yellow/green light. The combination of the blue, green and yellow lights appear white. An emission spectra should show two distinct peaks on either side of the visible spectra.

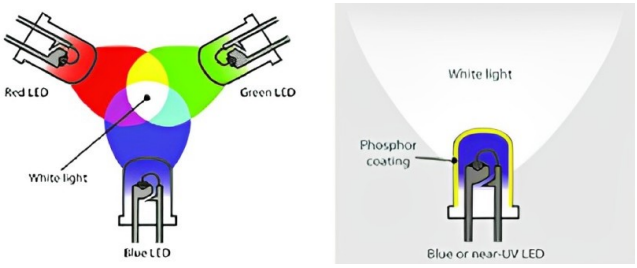

Figure 4: RGB colour mixing(left) and Phosphor converting(right) LEDs [6]

1.4.2 Infrared-emitting GaAs Diode

GaAs is a direct semiconductor with a numerically solved undoped band gap temperature dependence of

$$E_{gd}(T) = 1.52 - \frac{5.9 \times 10^{-4} \times T^2}{T + 300} \tag{9}$$

where E_{gd} is measured in eV and T in Kelvin. At room temperature, the band gap has a width of 1.4 eV which is in the infrared range. The reason for the temperature dependence of E_{gd} is the temperature dependence of atomic positions [4]. As the atomic positions change, the overlap of the electron wave functions change, altering the width of the forbidden energy band. If the emitted light has energy close to the band gap, some of it will be reabsorbed for band-to-band transitions. This will reduce the efficiency of the diode. In order to combat this, Si is introduced as an amphoteric defect that act as a donor when replacing Ga sites, and an acceptor when replacing As sites. For a high Si concentration, the discrete defect levels get broadened into impurity bands that overlap with the valence and conduction bands. These energy states in the band gap that continuously connect the band edges are called band tails. These reduce the width of the band gap which leads to luminescence at longer wavelengths. Equation (9) is adjusted to

$$E_{gd}(T) = 1.519 - \frac{5.404 \times 10^{-4} \times T^2}{T + 204} \tag{10}$$

1.4.3 Red-emitting Ga(As, P) Diode

GaP has a band gap corresponding to 546 nm at room temperature, which is the visible red range. However, the indirect band structure makes the transition probabilities very low due to the requirement of a phonon. To address this challenge, one approach is to amalgamate GaP with a direct semiconductor such as GaAs, thus creating an alloy $GaAs_{1-x}P_x$ where x is the molar ratio of phosphorus and arsenic. Numerically solved dependencies on x for the direct E_{gd} and indirect E_{gi} transition energies yield [4]:

$$\begin{aligned} E_{gd}(x) &= E_{gd}(0) + [E_{gd}(1) - E_{gd}(0) - 0.23]x + 0.23x^2 \\ E_{gi}(x) &= E_{gi}(0) + [E_{gi}(1) - E_{gi}(0) - 0.23]x + 0.23x^2 \end{aligned} \tag{11}$$

Values of E_{gd} and E_{gi} for $x = 0$ and $x = 1$ are known from [4]:

Material	Band Gap (eV) T = 300K
GaAs	$E_{gd}(0) = 1.43$
	$E_{gi}(0) = 1.82$
GaP	$E_{gd}(1) = 2.781$
	$E_{gi}(1) = 2.272$

We can identify an intersection x_s, between the transition energies. Below this threshold, the semiconductor behaves as a direct semiconductor, while above it, it exhibits characteristics of an indirect semiconductor.

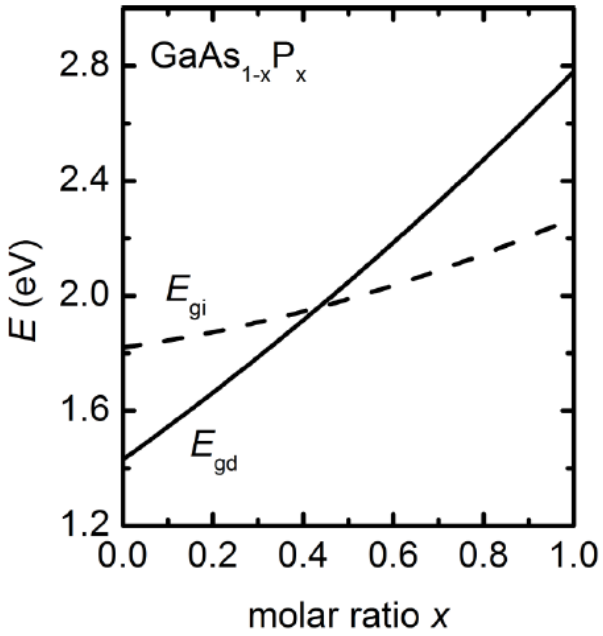

Figure 5: Dependence of band gaps on molar ratio x in $GaAs_{1-x}P_x$ [4]

We choose a molar ratio slightly below x_s, such that we have a direct semiconductor that emits red light, portraying a conduction band to acceptor event:

$$E_{max} = E_{gd}(x) - E_A \tag{12}$$

1.4.4 Yellow-emitting Ga(As, P) Diode

Choosing a higher GaP concentration in the alloy, such that $x > x_s$ will yield an indirect semiconductor corresponding to lower transition probability. We choose here $x = 0.87$. A nitrogen dopant is introduced to address this issue, creating isoelectronic defects. These defects will localise the wave functions increasing momentum uncertainty. This leads to transitions occurring without the necessary phonon contribution, increasing the overall transition probability. The radiation emitted is due to an exciton bounded to an isoelectronic defect such that:

$$E_{max} = E_{gi}(x) - E_{ex} - E_B \tag{13}$$

where E_B is the exciton binding energy. One uses (11) to calculate $E_{gi}(x = 0.87)$ while E_{ex} is known from [4].

1.4.5 Green-emitting GaP diode

Again, an indirect GaP semiconductor doped with nitrogen is used. By introducing nitrogen to phosphorus sites, we create isoelectronic defects that make transitions possible without additional phonon interactions as already mentioned. The emission spectrum will depend significantly on dopant concentration and temperature. Even though we perform the analysis at room temperature, three distinct cases must be taken into account:

- Low [nitrogen], very low T ($\approx 4.2K$): Two distinct lines will appear. The first being due to recombination of an exciton bound to an isolated N defect, and the second from the same recombination but with an additional phonon creation during the process. A part of the energy released during recombination is manifested in the form of a phonon, altering (13) to

$$E_{max} = E_{gi}(x) - E_{ex} - E_B - E_{ph} \tag{14}$$

- High [nitrogen], very low T: One line appears due to excitons bound to nitrogen pairs recombining.
- High [nitrogen], high T: Due to brand broadening, a line spectrum can no longer be resolved. Similar to the the yellow diode, we use (13) to calculate average exciton binding energy.

1.4.6 Blue-emitting SiC diode

We require here a dopable material that has a bandgap larger than 2.5eV. SiC can have different crystal structures such as cubic, hexagonal or rhombohedral, leading to different indirect band gaps. Accurate ideas about the recombination mechanism do not exist in current research [4].

1.5 Photoluminescence of $Ga_{1-x}Al_xAs$ sample

In the previous sections, we pushed our samples out of equilibrium by providing an electric potential difference. We now emit photons onto two unintentionally doped samples of $Ga_{1-x}Al_xAs$ to study emission spectra that will help us determine the bandgap types, and make an estimate for the molar ratio x. For $x > 0.45$, the sample switches from a direct to an indirect semiconductor changing the types of recombination events severely. From [4] we see the alloy band gap to be

$$E_{gd}(x,T) = E_{gd}(GaAs,T) + 1.42x \tag{15}$$

where $E_{gd}(GaAs,T)$ is given by (10). Due to a thermal distribution of charge carriers, the maximum of the band-to-band recombination will be given by:

$$E_{max} = E_{gd}(x,T) + \frac{k_B T}{2} \tag{16}$$

2 Experimental Setup

The arrangement to record luminescence spectra is shown below:

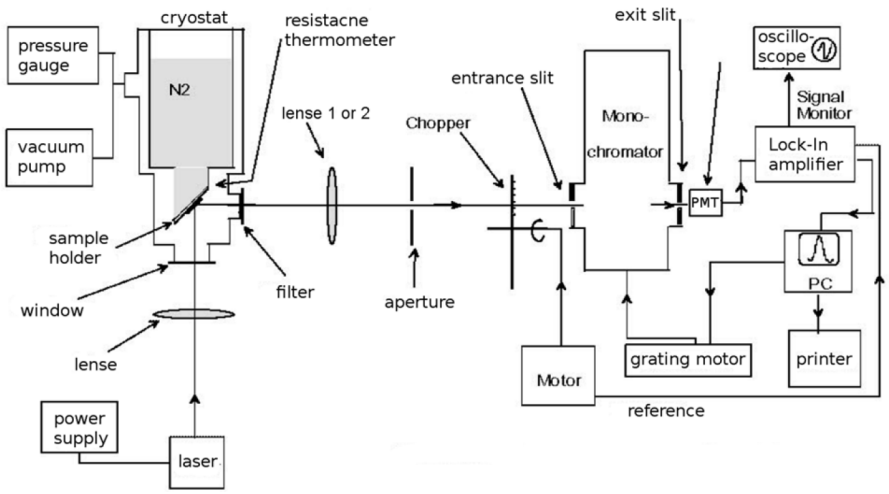

Figure 6: Experimental setup for electro- and photoluminescence [4]

We aim to measure the luminescence spectrum of a sample both at room temperature and close to liquid nitrogen temperature (approximately 87 K). The sample is placed in the cryostat's holder, and its temperature is monitored using a Pt resistance thermometer. Luminescence diodes and a Na vapor lamp, utilized for measurement purposes, are positioned in front of the cryostat.

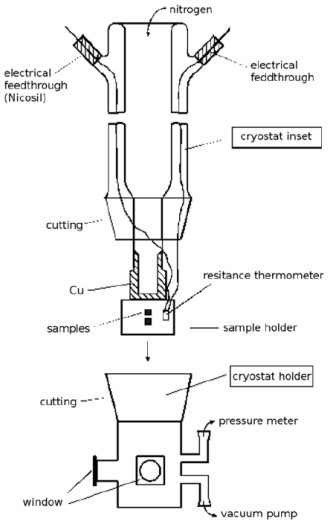

Figure 7: Schematic view of the cryostat [4]

To minimize heat exchange with the environment inside the cryostat during

cooling, we evacuate it using a rotary vane vacuum pump. A vacuum gauge indicates the pressure inside. Our excitation source is a diode laser and a Nd:YAG laser which emit wavelengths of 808 nm and 1064 nm respectively. Due to frequency doubling, the final emission will have a wavelength of 532 nm.

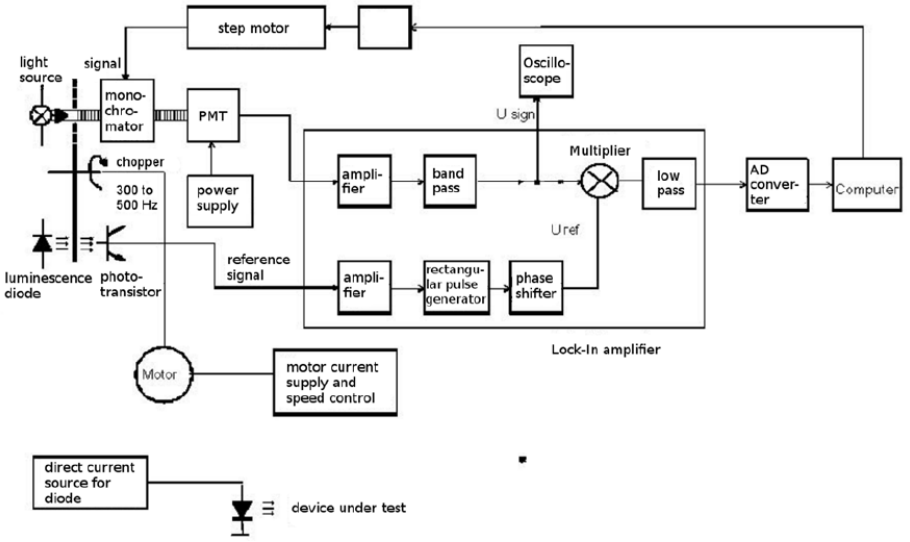

Figure 8: Schematic view of detection system [4]

The luminescence radiation emitted by the sample is directed through a filter, aperture, and quartz lens to the entrance slit of a SP-2155 grating monochromator, where it is spectrally decomposed using a grating. An optical chopper in front of the monochromator interrupts the radiation periodically, typically at a frequency of 300 to 500 Hz to improve signal-to-noise ratio. The reference signal from the chopper is also necessary for phase-sensitive detection. The monochromatic light passes through the exit slit onto a photo-multiplier tube (PMT). The PMT converts the alternating light into an alternating current of the same frequency, which is then analyzed using phase-sensitive lock-in amplification. The PMT however, has a limited efficiency (the ratio of electrons it actually releases to the photons it is able to pick up), which is highly dependent on the wavelength. The exact ratio Q is called quantum efficiency and illustrated in 9. In our setup we utilized the R298 photo-multiplier tube.

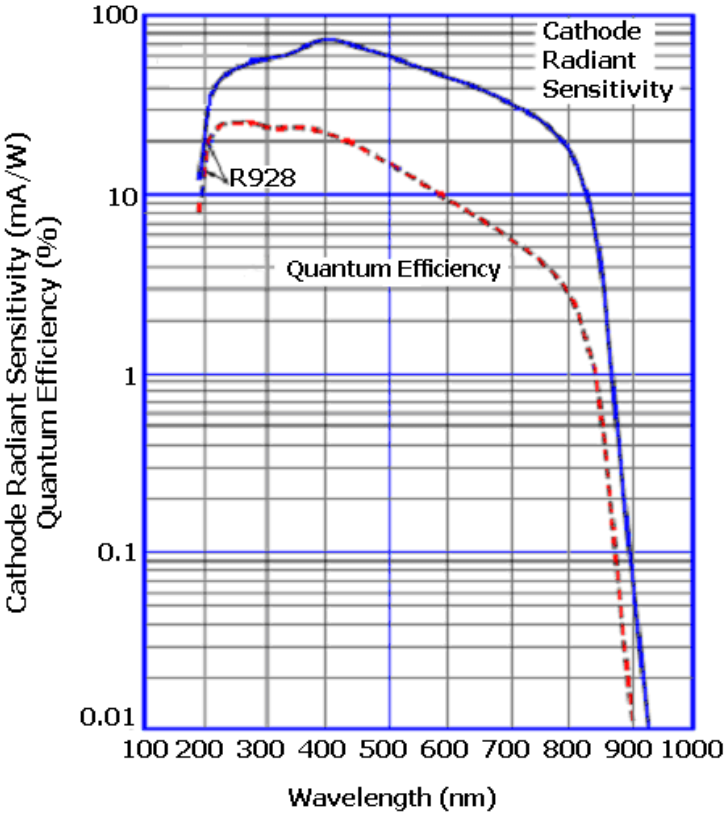

Figure 9: Quantum efficiency for R298 PMT [7]

As we will see in one of the tasks, when measuring emission spectra in the infrared region, the quantum efficiency will play an imperative role. The reference signal and the PMT signal are multiplied together to give us the final voltage which is sent to our computer via an AD-converter.

3 Results & Discussion

3.1 Emission Spectra of Sodium

The aim of this first task is to calibrate our setup by comparing the wavelength profile of a sodium lamp against the well known characteristic lines of sodium. To that end we measure the spectra around the 597, 819, and 497 nm lines and analyze the results. For all the measurements we keep a slit width of $10\mu m$. The step length used is $0.02nm$

3.1.1 597 nm lines

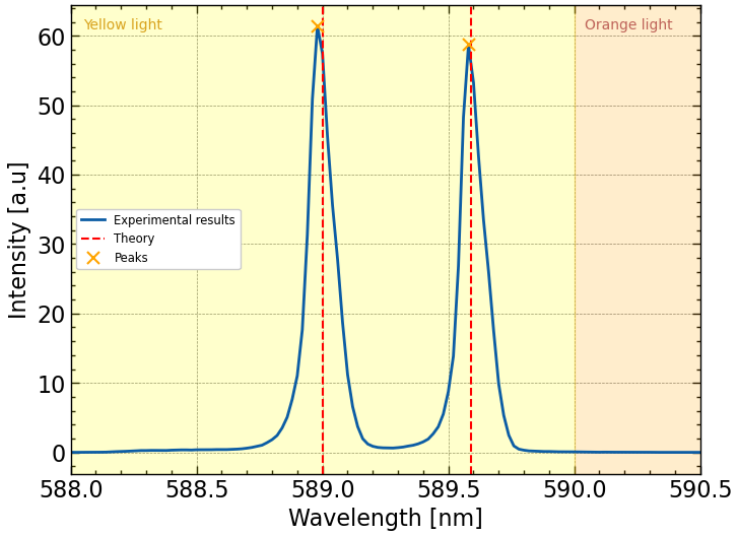

Figure 10: Wavelength profile of a sodium vapor lamp around 597 nm

We find that:

Theoretical Peak (nm)	Experimental Peak (nm)	Associated FWHM (nm)
589.00	588.98 $\pm$0.02	0.12 $\pm$0.04
589.59	589.58 $\pm$0.02	0.12 $\pm$0.04

The first peak gives us a relative error of 0.003%, and the second one of 0.002%. The FWHM measurements are appropriate in the context of the resolution of the monochromator for a slit width of $10\mu m$, which is $0.1nm$.

3.1.2 819 nm lines

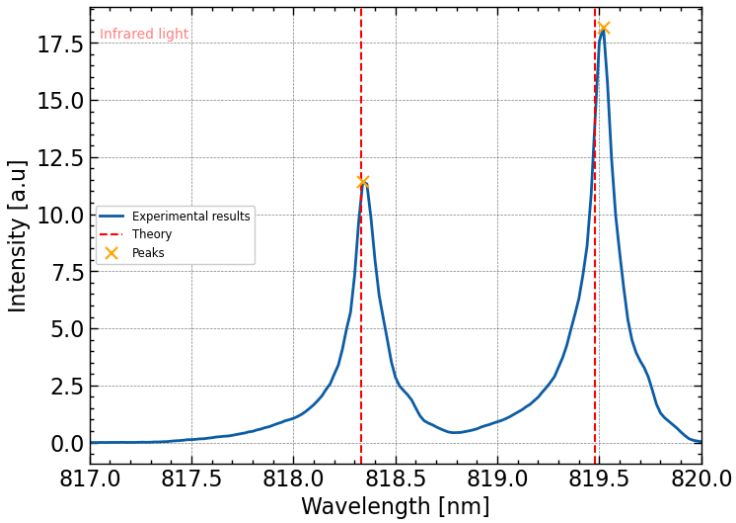

Figure 11: Wavelength profile of a sodium vapor lamp around 819 nm

We find that:

Theoretical Peak (nm)	Experimental Peak (nm)	Associated FWHM (nm)
818.33	818.34 ±0.02	0.16 ±0.04
819.48	819.52 ±0.02	0.16 ±0.04

The first peak gives us a relative error of 0.001%, and the second one of 0.005%. The FWHM measurements are, once again, in an acceptable range.

3.1.3 497 nm lines

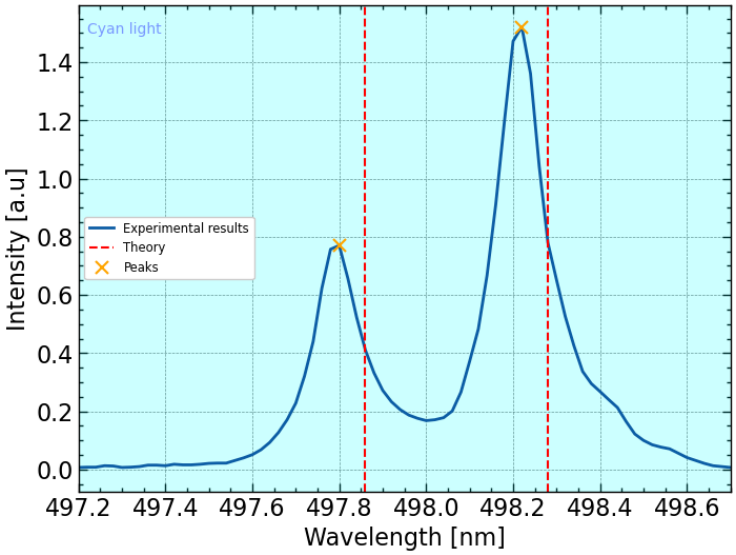

Figure 12: Wavelength profile of a sodium vapor lamp around 497 nm

For the third doublet, we find:

Theoretical Peak (nm)	Experimental Peak (nm)	Associated FWHM (nm)
497.86	497.80 ±0.02	0.12 ±0.04
498.28	498.22 ±0.02	0.14 ±0.04

The first peak gives us a relative error of 0.01%, and the second one of 0.01%. These are substantially higher than our previous measurements but still in an acceptable range. The FWHM measurements are still consistent with respect to previous lines.

Taking an average of all the relative errors, we establish a mean relative error of our setup of around:

$$\langle \mathrm{RE} \rangle = \frac{\sum_i \mathrm{RE}_i}{6} = 0.005\% \tag{17}$$

3.2 Luminescence Spectra of a White Light Emitting Diode

We record the wavelength profile of a white light emitting diode. We use a slid width of $10\mu m$ and a step length of 1 nm. A sensitivity of 50mV was considered suitable for the lock-in amplifier.

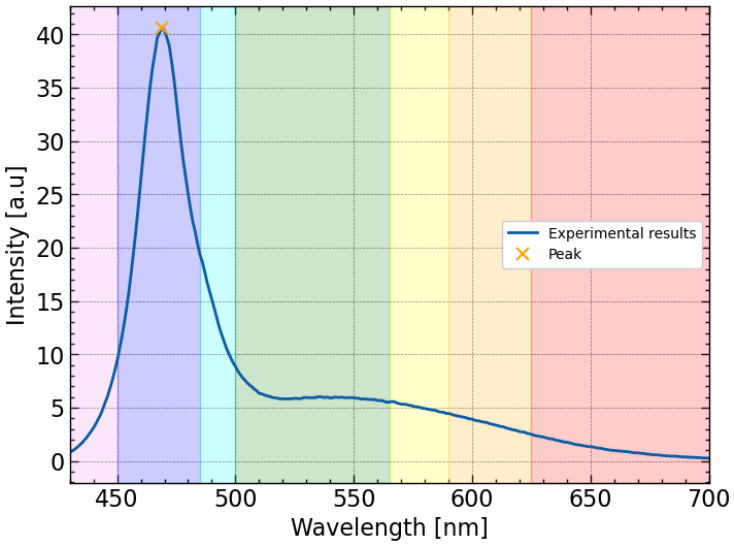

Figure 13: Wavelength profile of a white light emitting diode

We see that the white light peaks in the blue part of the spectrum at 469 nm with non-zero contribution from the rest, especially in the green/yellow region. As mentioned in 1.4.1, this gives us insights onto the inner workings of the LED. We conclude that we are dealing with a **phosphor converting diode**. The peak in the blue originates from the excitation source of the phosphor, which in turn contributes to the plateau in the 500 to 600 nm range.

3.3 Luminescence Spectra of a Blue Light Emitting Diode

In this section we recorded the wavelength profile of a blue light emitting diode. Due to the reduced inherent intensity of the blue diode, we increased the slid width to $50\mu m$ as per instruction, but kept a step length of 1 nm. This corresponds to an absolute error of ± 1 nm.

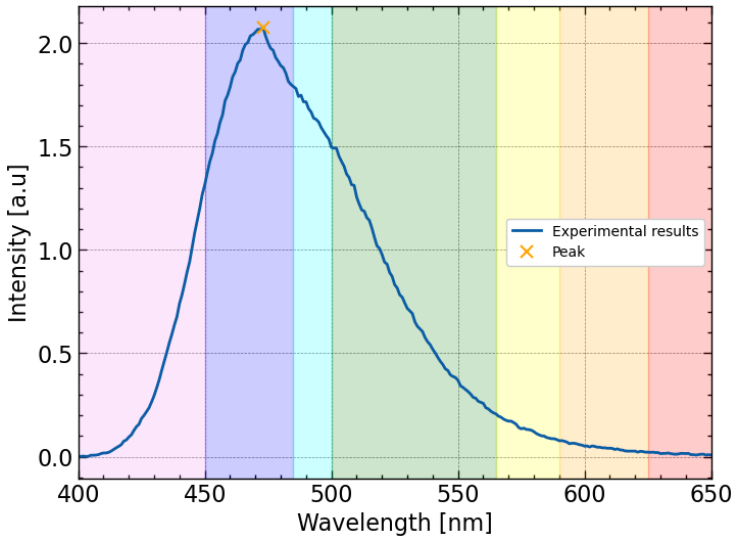

Figure 14: Wavelength profile of a blue light emitting diode

The result is in agreement to the theory, with $\lambda_{\max} = 473 \pm 1$ nm. The most intense wavelength, and as such, the main contributor to the emitted light, is found in the blue region of the spectrum.
Even though the exact recombination mechanisms of SiC diode is unknown, a broad spectral width can be a possible outcome of having a large band gap which may lead to a broader range of transition energies.

3.4 Luminescence Spectra of a Green Light Emitting Diode

We now record the wavelength profile of an indirect semiconductor GaP. The phosphorus site is doped with nitrogen, which causes the isoelectronic defects. The slid width used is $30\mu m$ but the step length remains unchanged.

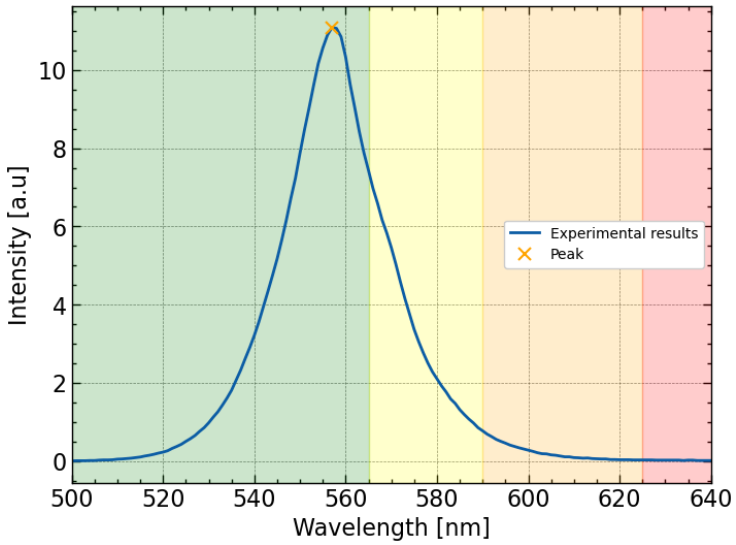

Figure 15: Wavelength profile of a green light emitting diode

The peak wavelength is at $\lambda_{max} = 557 \pm 1$ nm, as expected from the green region of the spectra. Given that the measurement was taken at room temperature, no degeneration must be taken into account and the emitted radiation will be solely due to isoelectronic defects. To determine the exciton binding energy E_B we use (13) and consider E_{gi} well known, with only a temperature dependence:

$$E_B = E_{gi}(T) - E_{ex} - E_{max} \tag{18}$$

With:

- $E_{gi}(T = 300K) = 2.272\,eV$ [4]
- $E_{ex} = 0.022\,eV$, using (7) with $m_p = 0.5$m and $m_n = 0.35$ m
- $E_{max} = \frac{hc}{\lambda_{max}} = 2.226 \pm 0.004\,eV$

This yields a binding energy of:

$$E_B = 0.024 \pm 0.004\,eV \tag{19}$$

3.5 Luminescence Spectra of a Yellow Light Emitting Diode

As previously discussed in 1.4.4, yellow light emitting diodes are usually a combination of GaP indirect semiconductors, mixed with a direct semiconductor of $GaAs$ alloy, thus obtaining $GaAs_{1-x}P_x$. With the molar ratio being $x = 0.87$, the the semiconductor remains an indirect one. The phosphorus site is also doped with nitrogen, which causes the isoelectronic defects. The slid width used and the step length remain unchanged.

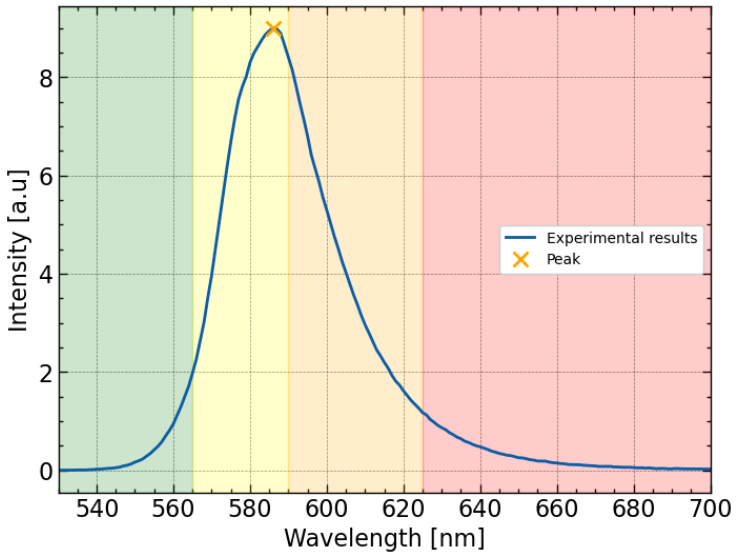

Figure 16: Wavelength profile of a yellow light emitting diode

The peak is found in the yellow region of the spectrum at $\lambda_{max} = 586 \pm 1$ nm, which corresponds to a maximum energy of: $E_{max} = \frac{hc}{\lambda_{max}} = 2.116 \pm 0.004\, eV$. To find E_B, we use equation (13), with the same $E_{ex} = 0,022\, eV$.

However, E_{gi} presents a molar ratio dependence such that: $E_{gi} \equiv E_{gi}(x)$. From equation (11):

$$E_{gi}(x) = E_{gi}(0) + [E_{gi}(1) - E_{gi}(0) - 0.23]x + 0.23x^2 \tag{20}$$

With $E_{gi}(0) = 1.82\, eV$, $E_{gi}(1) = 2.272 e\, V$ and $x = 0.87$, we find that $E_{gi}(x = 0.87) = 2.187\, eV$. From (13) we find that our binding energy this time is:

$$E_B = 0.049 \pm 0.004\, eV \tag{21}$$

3.6 Luminescence Spectra of a Red Light Emitting Diode

As discussed in 1.4.3, our $GaAs_{1-x}P_x$ sample has a molar ratio slightly below x_s such that we have a direct semiconductor that emits red light. This assures appropriate energy gap as well as high transition probability. The slid width for the following measurements remains $30\mu m$ and the step length 1 nm.

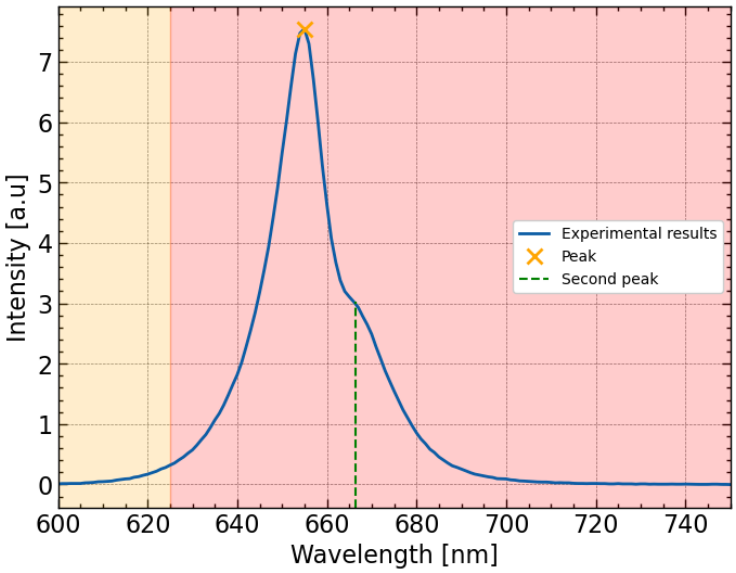

Figure 17: Wavelength profile of a red light emitting diode

The intensity maximum is at $\lambda_{max} = 655 \pm 1$ nm, which corresponds to a maximum energy of: $E_{max} = \frac{hc}{\lambda_{max}} = 1.893 \pm 0.004\, eV$.
A conduction band to acceptor event will obey (12). The ionisation energy of the acceptor can be approximated using a hydrogen-like model:

$$E_A = \frac{13.6 m_p}{\epsilon^2 m} \text{eV} \tag{22}$$

where m_p is the effective mass of a hole. From [4], we set $m_p = 0.5m$, and $\epsilon = 12.9$ which yields $E_A = 0.041$ eV.
We can now estimate the band gap $E_{gd}(x)$ as per (12) to be,

$$E_{gd}(x) = 0.041\text{eV} + (1.893 \pm 0.004)\text{eV} = 1.934 \pm 0.004\text{eV} \tag{23}$$

In order to calculate the molar ratio, we refer to (11) and [4], from which $E_{gd}(0) = 1.43$ eV and $E_{gd}(1) = 2.781$ eV thereby yielding

$$\begin{aligned} (1.934 \pm 0.004) &= 1.43 + (2.781 - 1.43 - 0.23)x + 0.23x^2 \\ \implies x &= 0.414 \pm 0.006 \end{aligned} \tag{24}$$

The error in x was calculated using upper and lower bound of $E_{gd}(x)$. The arsenic content is simply $1 - x = 0.586 \pm 0.006$.
In order to check the validity of our x value, we make a theoretical estimate of x_s using values found in [4] such that $E_{gd}(x) = E_{gi}(x)$

$$\begin{aligned} \implies & E_{gd}(0) + [E_{gd}(1) - E_{gd}(0) - 0.23]x + 0.23x^2 \\ & = E_{gi}(0) + [E_{gi}(1) - E_{gi}(0) - 0.23]x + 0.23x^2 \end{aligned} \tag{25}$$

which yields the intersection $x_s = 0.434 > x$.

Additionally, at approximately $\lambda = 665.5 \pm 1$ nm, with an intensity that is $\approx 40\%$ of the maxima, we notice a small protrusion that seems to indicate the

presence of a possible second peak. Given that we have a conduction to acceptor recombination, a secondary lower energy radiation may be due to an exciton with a light hole [8]. Due to spin-orbit interaction of the involved atomic states, the degeneracy of the valence band is lifted, and we have heavy and light hole branches. Due to different parabolicity, the holes have different effective masses $m^* = \hbar^2 \left(\frac{d^2E}{dk^2}\right)^{-1}$.

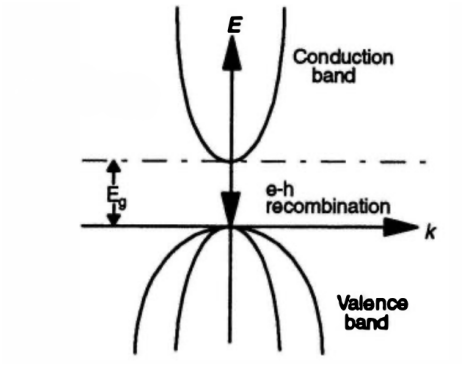

Figure 18: Valence Band Split depicting Heavy (top) and Light (bottom) holes

The lower effective mass causes the radiated photon to have lower energy as shown from the spectra. It can be concluded that the light hole exciton experienced an effective mass μ^*_{lh} such that $\mu^*_{lh} = 0.4\mu^*_{hh}$.

3.7 Luminescence Spectra of an Infrared Light Emitting Diode

The last LED analyzed was the GaAs direct semiconductor, the theory of which has been covered in 1.4.2.

As per instructions, the slit width was increased to $200\mu m$ to compensate for low luminosity, and step length kept at 1 nm.

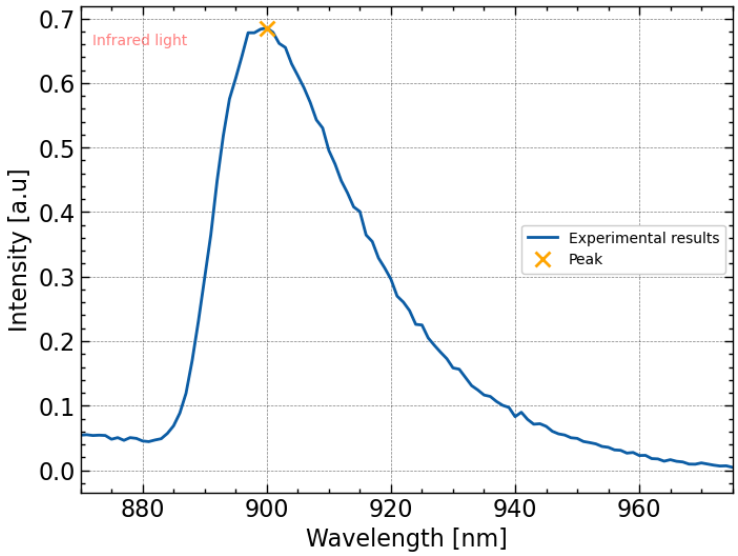

Figure 19: Wavelength profile of a infrared light emitting diode

The experimental peak is found at $\lambda_{max} = 900 \pm 1$ nm, however we know from [4] that we are dealing with a GaAs diode with center wavelength of about 940 nm at $T \approx 300K$. As suggested from the task itself, we see that the PMT in use (as discussed in Section 2) has issues detecting photons with λ higher than 900 nm, as per figure 9. Its efficiency decreases considerably, which explains the discrepancy in our measurement. Due to the inherently low luminosity of the diode, the lockin-amplifer was set to a relatively low sensitivity of $(1mV)$, perfectly representing the quick loss of information that is the result of a sharp decrease in Q.

Regardless, the associated E_{max} to our recorded λ_{max} will be: $E_{max} = (1.378 \pm 0.004)eV$.

The energy band gap E_{gd} for an infrared-emitting GaAs diode doped with silicon is described in equation 10. For $T = 300K$ we find:

$$E_{gd}(T) = 1.519eV - \frac{5.404 \times 10^{-4} \times (300)^2}{(300) + 204} eV = 1.423eV \tag{26}$$

This is $(0.045 \pm 0.004)eV$ higher then what we found experimentally. If, as per the task suggestion, we calculate ionization energies of donors and acceptors using equations 5 and 6, with the effective mass of the electron $m_n = 0.067m$, and the effective mass of a hole $m_p = 0.5m$ [4], we find that:

- $E_{donor} = 0.005$ eV
- $E_{acceptor} = 0.041$ eV

We can see that the ionization energy combined seem to equal the difference between our experimental energy maxima and the theoretical energy band gap E_g. This makes sense, considering that the doping agent Si in this diode, which acts both as a donor (on Ga sites) and an acceptor (on As sites), is the reason of the ionization energies. This hints at a high concentration of the doping agent, coupled with a loss of quantum efficiency.

3.8 Temperature Dependent Luminescence Spectra of Two AlGaAs Samples

We measured the spectra of two $Al_{1-x}Ga_xAs$ samples with two different compositions, at room temperature and at $T \approx 86.65 \pm 0.5$ K with a fluctuation of ± 0.5 K during the data recording. The lab codes for the samples are as follows - Sample 1: 87063 and Sample 2: 1127.

Sample	Slit Width (μm)	Sensitivity (mV)	Step length (nm)
1 (T = 300 K)	300	10	1
2 (T = 300 K)	300	1	1
1 (T = $86.65 \pm 0.5K$)	80	2	1
2 (T = $86.65 \pm 0.5K$)	80	0.5	1

The recorded spectra is presented below:

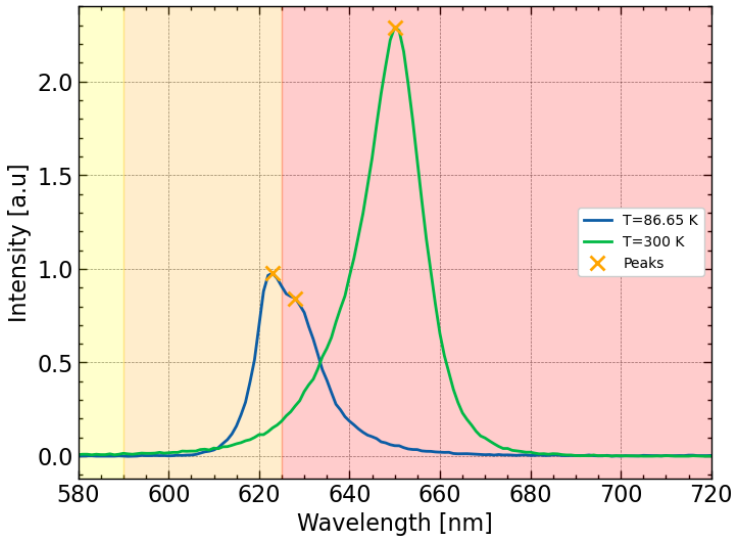

Figure 20: Wavelength profile of sample 1

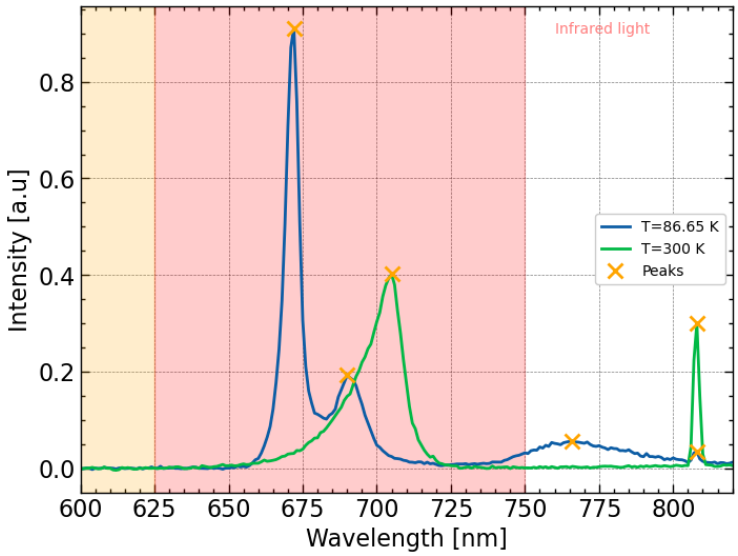

Figure 21: Wavelength profile of sample 2

The corresponding peaks are mentioned below:

Sample	Temperature (K)	Peaks (nm)
1	300	650 ± 1
	86.65 ± 0.5	623 ± 1, 628 ± 1
2	300	705 ± 1, *808 ± 1*
	86.65 ± 0.5	672 ± 1, 690 ± 1, 766 ± 1, *808 ± 1*

In order to refer to the peaks, we adapt the following notation: λ_{ijk} where i is the sample number, j the temperature, and k the peak number from the left. Immediately, one notices a strange common peak between the two sample 2 data sets $\lambda_{2,300,2}$ and $\lambda_{2,86.65,4}$. As most of the processes that result in emission have a dependency on temperature, having the exact same λ_{max} at drastically different temperatures, may suggest a systematic error. We thus shine the Nd:YAG laser (properties of which are mentioned in section 2) onto our PMT as best as we can, and obtain the following spectra:

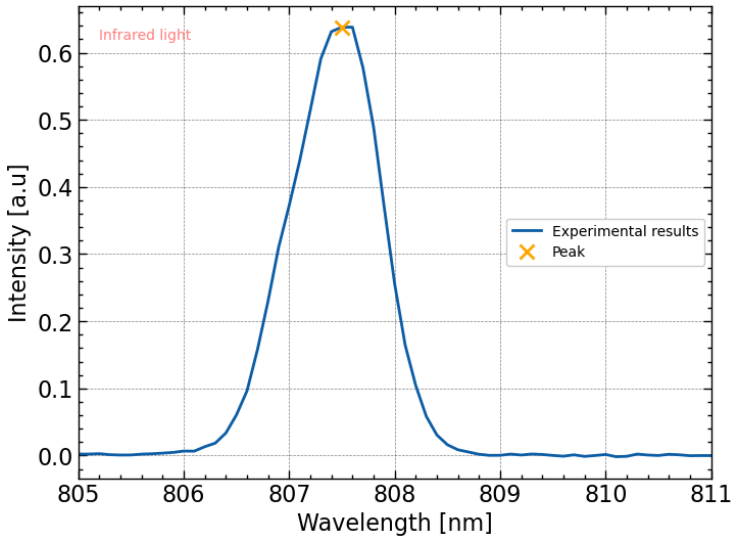

Figure 22: Wavelength profile of Nd:YAG laser

The measured peak is at 807.5 ± 0.5nm. Documentation shows that the diode laser emits at a wavelength of about 808 nm, we will thus eliminate $\lambda_{2,300,2}$ and $\lambda_{2,86.65,4}$ from further analysis.
The corresponding energies are as follows:

Sample	Temperature (K)	Peaks (eV)
1	300	1.907 ± 0.004
	86.65 ± 0.5	1.990 ± 0.004, 1.974 ± 0.004
2	300	1.759 ± 0.004
	86.65 ± 0.5	1.845 ± 0.004, 1.797 ± 0.004, 1.619 ± 0.004

As mentioned in section 1.5, we now calculate the energy gap $E_{gd}(x,T)$ associated with the maximum of the recombination band using (16). Note that E_{max} will correspond to the highest peak for each spectra. The higher error for the cold measurements are a result of the uncertainty in temperature.

Sample 1 (ev)	Sample 2 (eV)
$E_{gd}(x_1, 300) = 1.8945 \pm 0.004$	$E_{gd}(x_2, 300) = 1.7457 \pm 0.004$
$E_{gd}(x_1, 86.65 \pm 0.5) = 1.9864 \pm 0.026$	$E_{gd}(x_2, 86.65 \pm 0.5) = 1.8413 \pm 0.026$

We notice an increase in the direct band gap with a drastic decrease in the temperature. The trends with regard to the size of the band gap for III–V semiconductors can essentially be understood in terms of the bond strength, or lattice constant [1].

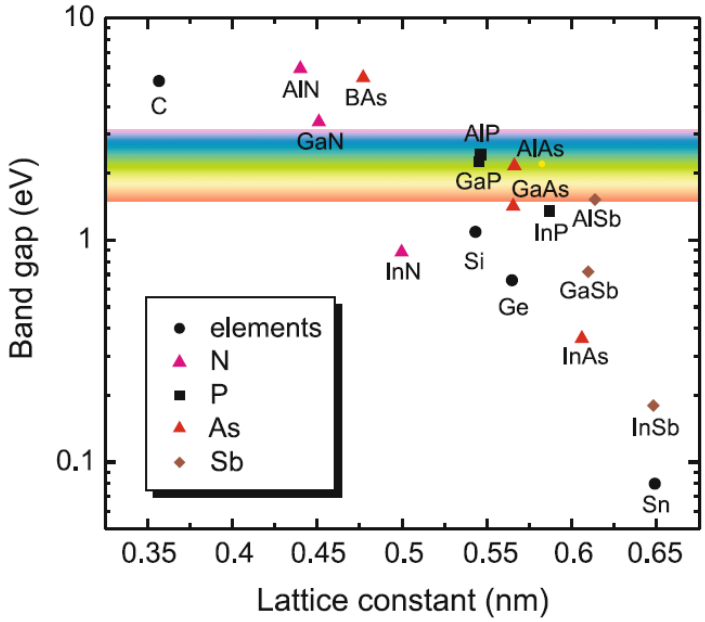

Figure 23: Band gaps as a function of the lattice constant for various elemental III–V semiconductors [1]

A detailed analysis of lattice constant dependence on band gap can be done using the Kronig-Penney model where a series of potential wells are used to compute electronic behaviour in a lattice. However, the essence of the physics is tied to a decrease in interatomic distances with lowered temperature. This increases the binding forces between valence electrons and parent atoms, thereby increasing the amount of energy required to convert them into conduction band electrons [9].
We now try to calculate the molar ratios of both samples using equation (15) where $E_{gd}(GaAs,T)$ will have the same temperature dependence as mentioned in (10). With $E_{gd}(GaAs, 300) = 1.4225$eV and $E_{gd}(GaAs, 86.65) = 1.505$eV, we

have the following molar ratios. The uncertainties of the avarge of the values are calculated as standard error of the means.

Sample 1	Sample 2
$x_{1,300} = 0.332 \pm 0.003$	$x_{2,300} = 0.228 \pm 0.003$
$x_{1,86.65\pm0.5} = 0.339 \pm 0.018$	$x_{2,86.65\pm0.5} = 0.237 \pm 0.018$

$$\implies \langle x_1 \rangle = 0.336 \pm 0.009 \qquad \langle x_2 \rangle = 0.232 \pm 0.009$$

We note that both samples are direct semiconductors with $x < 0.45$ [4].

One major qualitative confirmation is the 'bump' to the right of the first peak in sample 1 as seen in figure 20 within the low temperature regime. With the sample being the one with highest Ga concentration, it showed most similar behavior to the infrared diode in section 3.6.

In order to judge the spectral purity of the emissions, we analyse the dependence of the FWHM on temperature. Due to thermal distribution, the ideal half-width of the bands are expected to be $1.8k_BT$. The values for the context of a step length of 1 nm are the following:

	FWHM (nm)		
Sample 1(87063)(T= 300 K)	15 ± 1		
Sample 2(1127) (T=300 K)	15.5 ± 1		
Sample 1 (87063) ($T = 86.65 \pm 0.5K$)	16 ± 1		
Sample 2(1127)($T = 86.65 \pm 0.5K$)	5.5 ± 1	14 ± 1	8 ± 1

For sample 1 we note that there has only been a change of $1nm$ for the half-width with such a drastic change in temperature. This is due to the secondary $\lambda_{1,86.65,2}$ peak that remains unresolved at our step width. We would require high-resolution spectroscopy for further analysis. In sample 2 however, for the first peak we notice a decrease in FWHM by 10 nm with the drop in temperature. We can verify that this is in perfect accordance to the theory:

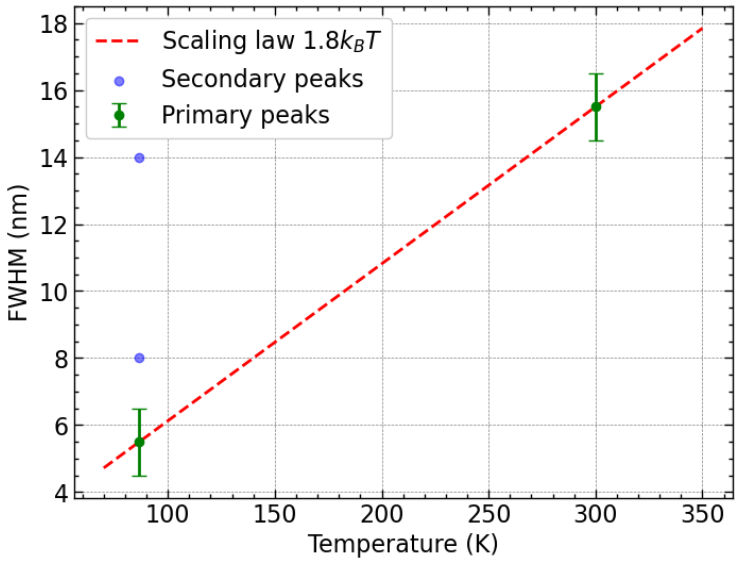

Figure 24: FWHM increase with temperature compared to its scaling law

A general trend of broader spectral features can be noticed among both the samples as temperature is increased. The distinct heavy and light-hole peaks in both samples become completely unresolved into one broad peak at 300K. Sample 2 being the one with the lowest molar ratio, portrayed very distinct peaks at 86.65K. Generally, as thermal energy is decreased, carriers experience fewer scattering events leading to more pronounced luminescence peaks.

4 Conclusion & Outlook

In task 1, we established a relative error of 0.005% for the sodium lamp peaks, laying a satisfactory foundation for the rest of the report.
In task 2, we successfully inferred manufacturing details regarding the white LED solely from its emission spectra.
Due to the lack of a theoretical foundation about exact recombination processes for the SiC diode in task 3, further analysis was not conducted. However, we do note that SiC had the broadest FWHM out of all the diodes. This can be owed to SiC having various polytypes with different stacking sequences and electronic properties which lead to varying defect configurations [10].
In task 4 and 5, indirect semiconductors such as nitrogen doped GaP and alloy GaAsP were studied respectively. Using a predetermined bowing parameter equation from [4], we calculated exciton binding energies.
In task 6, the GaAsP alloy was again studied in the form of a red LED to determine the arsenic content, and switching ratio x_s. We also commented on the unresolved secondary peak due to light holes.
As the PMT had a very low efficiency above 900nm, task 7 provided unreliable data. Band gap and ionisation energies of donors and acceptors were still calculated for completion. We noted that $E_{donor} + E_{acceptor} \approx E_{gd}(T) - E_{max}$, which hinted at a high Si doping concentration.

The two samples in task 8 had molar ratios that differed by $\approx 31\%$. Even though both were still in the direct semiconductor regime, they presented very different luminescence behaviors. A comparison of FWHM of multiple peaks was conducted to facilitate a quantitative analysis. However, due to unresolved peaks in sample 1, the thermal dependency of FWHM was only verified for the second sample. As a recommendation for future investigations, we propose fitting the spectrum with multiple Gaussian or Lorentzian functions to deconvolute the peaks.
In addition to higher resolution spectroscopy, we also propose time-resolved spectroscopy [11] that will enhance our understanding of carrier lifespan and non-radiative recombination pathways, especially for indirect samples.

References

[1] Grundmann, M. (2016). *The Physics of Semiconductors*. Springer

[2] Kreher,K.: Festkörperphysik. Akademie-Verlag, Berlin 1973

[3] Harker,A.H.: TIGHT BINDING MODEL Lecture 20, Physics and Astronomy UCL

[4] Volker Riede; Wolfram Frizsche, Advanced Laboratory Guide, University of Leipzig

[5] Cabrera, Rowan (2019). Electronic Devices and Circuits. EDTECH

[6] Dutta Gupta, S., Agarwal, A. (2017). Artificial Lighting System for Plant Growth and Development: Chronological Advancement, Working Principles, and Comparative Assessment. Springer

[7] Jameson, David and Terpetschnig, Ewald. Fluorescence: Basic Instrumentation.

[8] Wójcik-Jedlińska, Anna; et al. (2009) Photoluminescence characterization of AlGaAs/GaAs test superlattices used for optimization of quantum cascade laser technology

[9] Parker, Greg. Introductory Semiconductor Device Physics (1994)

[10] J.F. Kelly; et al. (2005). "Correlation between layer thickness and periodicity of long polytypes in silicon carbide"

[11] Helmholtz-Zentrum Berlin für Materialien und. “Time-Resolved Spectroscopy.”